



HAL
open science

Hydrothermal synthesis of (Zr,U)SiO₄: an efficient pathway to incorporate uranium into zircon

Paul Estevenon, Thomas Barral, Arthur Avallone, Mateo Jeffredo, Alexis de la Hos, Andrew Strzelecki, Xavier Le Goff, Stephanie Szenknect, Kristina Kvashnina, Philippe Moisy, et al.

► To cite this version:

Paul Estevenon, Thomas Barral, Arthur Avallone, Mateo Jeffredo, Alexis de la Hos, et al.. Hydrothermal synthesis of (Zr,U)SiO₄: an efficient pathway to incorporate uranium into zircon. Dalton Transactions, 2024, 53 (33), pp.13782-13794. 10.1039/D4DT01604A . hal-04704276

HAL Id: hal-04704276

<https://hal.science/hal-04704276v1>

Submitted on 25 Oct 2024

HAL is a multi-disciplinary open access archive for the deposit and dissemination of scientific research documents, whether they are published or not. The documents may come from teaching and research institutions in France or abroad, or from public or private research centers.


L'archive ouverte pluridisciplinaire **HAL**, est destinée au dépôt et à la diffusion de documents scientifiques de niveau recherche, publiés ou non, émanant des établissements d'enseignement et de recherche français ou étrangers, des laboratoires publics ou privés.



Distributed under a Creative Commons Attribution 4.0 International License

Cite this: *Dalton Trans.*, 2024, **53**, 13782

Hydrothermal synthesis of (Zr,U)SiO₄: an efficient pathway to incorporate uranium into zircon†

Paul Estevenon, ^a Thomas Barral, ^b Arthur Avallone, ^b Mateo Jeffredo, ^b Alexis De La Hos, ^b Andrew Strzelecki, ^{c,d,e} Xavier Le Goff, ^b Stephanie Szenknect, ^b Kristina Kvashnina, ^{f,g} Philippe Moisy, ^a Renaud Podor, ^b Xiaofeng Guo ^{c,d,e} and Nicolas Dacheux ^{*b}

The preparation of synthetic (Zr,U)SiO₄ solid solution is challenging, as the conventional high-temperature solid-state method limits the solubility of uranium (4 ± 1 mol%) in the orthosilicate phase due to its thermodynamic instability. However, these compounds are of great interest as a result of (Zr,U)SiO₄ solid solutions, with uranium contents exceeding this concentration, being observed as corium phases formed during nuclear accidents. It has been identified that hydrothermal synthesis pathways can be used for the formation of the metastable phase, such as USiO₄. The investigation carried out in this study has indeed led to the confirmation of metastable (Zr,U)SiO₄ compounds with high uranium contents being formed. It was found that (Zr,U)SiO₄ forms a close-to-ideal solid solution with uranium loading of up to 60 mol% by means of hydrothermal treatment for 7 days at 250 °C, at pH = 3 and starting from an equimolar reactant concentration equal to 0.2 mol L⁻¹. A purification procedure was developed to obtain pure silicate compounds. After purification, these compounds were found to be stable up to 1000 °C under an inert atmosphere (argon). The characterisation methods used to explore the synthesis and thermal stability included powder X-ray diffraction (PXRD), Fourier transform infrared (FTIR) and Raman spectroscopies, scanning electron microscopy (SEM) and thermogravimetric analysis (TGA).

Received 2nd June 2024,
Accepted 23rd July 2024

DOI: 10.1039/d4dt01604a

rsc.li/dalton

1. Introduction

Zircon, ZrSiO₄, is a key mineral phase in geochronology because it is known to allow partial substitution of tetravalent zirconium (Zr⁴⁺) by tetravalent uranium (U⁴⁺), resulting in uranium contents typically ranging from 100 to 5000 ppm (ref. 1–5) and up to 11 mol% under very specific conditions.^{6,7} This phenomenon allows the use of U–Pb age determinations for zircon crystals, with ages that can exceed 4 billion years,^{8–11}

providing key information about the geological history of the Earth. Self-irradiation of zircon phases due to uranium decay causes metamictization,^{3,12–18} and the recovery of this radiation damage also provides key information about the history of metamorphic rocks.^{19–23} Both phenomena have been extensively studied because of their importance in geological and environmental sciences.

(Zr,U)SiO₄ phases are also of vital interest to nuclear science, as this species was identified as one of the predominant radioactive phases formed in corium during the Chernobyl nuclear accident.²⁴ Indeed, the accident that occurred in unit 4 of the Chernobyl nuclear power plant resulted in the melting of the nuclear fuel assemblies, which consisted of UO₂ and the zircaloy cladding material present in the reactor.^{20,25} The molten nuclear fuel assemblies then interacted with structural materials, consisting of concrete and stainless steel.^{24,26–28} In addition, materials were air dropped during the early stages of the accident including the silicate mineral serpentine and siliciclastic sand, lead boric acid, and dolomite, which in turn also interacted with the melted fuel.^{20,24–26} All this led to the formation of complex silicate melts, known as “Chernobyl lavas”, which penetrated and solidified in many areas under the reactor.^{24,26} The main uranium-bearing phases identified in these lavas are mixed

^aCEA, DES, ISEC, DMRC, Univ Montpellier, Marcoule, France^bICSM, Univ Montpellier, CNRS, CEA, ENSCM, Bagnols-sur-Cèze, France.

E-mail: nicolas.dacheux@umontpellier.fr; Tel: +33 4 66 33 92 05

^cDepartment of Chemistry, Washington State University, Pullman, Washington 99164, USA^dAlexandra Navrotsky Institute for Experimental Thermodynamics, Washington State University, Pullman, Washington 99164, USA^eMaterials Science and Engineering, Washington State University, Pullman, Washington 99164, USA^fHelmholtz Zentrum Dresden Rossendorf (HZDR), Institute of Resource Ecology, 01314 Dresden, Germany^gThe Rossendorf Beamline at ESRF–The European Synchrotron, 38043 Grenoble, Cedex 9, France† Electronic supplementary information (ESI) available. See DOI: <https://doi.org/10.1039/d4dt01604a>

uranium–zirconium oxide (U,Zr)O₂ and silicate (Zr,U)SiO₄ phases.²⁶ The (Zr,U)SiO₄ phases, sometimes referred to as “Chernobylite”,²⁹ have been observed to contain up to 12 mol% uranium.^{20,24,26,28–33} Similar (Zr,U)SiO₄ phases are expected for the Fukushima Daiichi accident due to similar phenomena of melted fuel interactions with structural materials.^{34,35} In addition, experiments simulating corium formation are also successful in forming (Zr,U)SiO₄ solutions.^{36,37}

From a chemical point of view, the formation of these phases is a result of the crystal chemistry of zircon-type silicate compounds.³⁸ In fact, it is known that tetravalent zirconium, hafnium, cerium and actinide (An) silicates (more precisely Th, Pa, U, Np, Pu and Am) crystallise in the same *I4₁/amd* crystal structure with the chemical formula MSiO₄.^{39–42} This behaviour allows the partial substitution of zirconium, at the A site of the zircon structure, with other tetravalent metal cations, such as uranium, in ZrSiO₄. In addition, zircon-type phases are very resistant to leaching under weathering conditions.^{43–49} These properties of long-term stability, very low leachability, and affinity for actinide has led to the proposal of (Zr,An)SiO₄ phases as potential actinide-specific solid waste forms for the long-term disposal of spent nuclear fuel.^{50–66}

However, attempts to synthesise (Zr,U)SiO₄ by conventional high-temperature solid-state methods have yielded very limited results, with the highest uranium concentration synthesized by this method being limited to 4 mol%.⁶⁷ In addition, the synthesis of pure silicate samples by this route is difficult and the samples obtained are usually mixtures of silicates and oxides. This solubility limitation can be explained by the ionic size difference between the Zr(IV) and U(IV) cations in octahedral coordination, 0.84 Å and 1.00 Å, respectively,⁶⁸ which induces important structural strains.^{69,70} Calculations performed on this system also predicted the thermodynamic instability of these solid solutions.⁷¹ Nevertheless, the existence of environmental and accidental samples above the solubility limit demonstrated the possibility of forming zircon with a higher uranium content due to specific stability conditions or kinetic pathways, and at least suggested the existence of metastable states allowing their observation. In this context, the preparation of representative and chemically pure uranium-doped zircon above the currently observed synthetic solubility limit of 4 mol% uranium is a challenge to evaluate its thermodynamic and chemical properties and long-term behaviour, both for the environmental aspect (actinide behaviour in silicate-rich geological conditions) and for the understanding of actinide-containing zircon-type solid nuclear wastes.

Hydrothermal synthesis has been considered as a potential method to circumvent this experimental lock, as hydrothermal synthesis routes have been demonstrated to obtain pure metastable silicate phases such as USiO₄ or CeSiO₄.^{42,72–79} In addition, the literature on the hydrothermal synthesis of the (Zr,U)SiO₄ solid solution has already reported the formation of metastable uranium-rich zircon compounds with up to 20 mol%^{69,80,81} and 27 wt% (*i.e.* 25 mol%) uranium according

to Ioudintsev *et al.*⁸² Based on recent progress in the synthesis of ZrSiO₄ and (Zr,Ce)SiO₄ phases,⁸³ the aim of this work is to revisit the solubility of uranium in ZrSiO₄ using the soft hydrothermal synthesis method.

2. Materials and methods

2.1. Syntheses

2.1.1. Preparation of (Zr,U)SiO₄. Natural uranium is an alpha particle emitter and is considered a health hazard. Experiments involving actinides require appropriate facilities and personnel trained in the handling of radioactive materials.

A 6 mol L⁻¹ HCl solution was prepared *via* dilution of 12 mol L⁻¹ HCl (37%) stock solution of ACS grade from Sigma-Aldrich. The uranium(IV) chloride mother solution used was prepared by dissolving metallic uranium chips in the 6 mol L⁻¹ HCl solution.⁸⁴ The concentration of the uranium(IV) solution was determined by inductively coupled-atomic emission spectroscopy (ICP-AES) to be $C_U = 0.62 \pm 0.01$ mol L⁻¹. All other reagents used were supplied by Sigma-Aldrich. Na₂SiO₃·5H₂O (≥95%) and ZrOCl₂·8H₂O (≥99%) were used to produce aqueous silicate and zirconium precursors, respectively. An 8 mol L⁻¹ NaOH solution was freshly prepared from Sigma-Aldrich ACS grade NaOH (98%) prior to the experiments.

Syntheses of (Zr,U)SiO₄ solid solutions were carried out under an air atmosphere based on the conditions identified in the previous work for the synthesis of ZrSiO₄⁸³ and the acidity conditions were expected to favour the formation of metal silicate gels with tetravalent metal ions⁸⁵ (*i.e.* to promote nucleation). Aqueous zirconium, uranium and silicate solutions were prepared by dissolving ZrOCl₂·8H₂O and Na₂SiO₃·5H₂O in aqueous HCl and then adding uranium solution to obtain a reacting mixture in 1 mol L⁻¹ HCl with a silicate excess of 5 mol%. A global cation concentration ($C_{Zr(IV)} + C_{U(IV)}$) at 0.2 mol L⁻¹ was considered, with different zirconium and uranium concentrations depending on the desired composition (Table SI 1†). The pH of the mixture was then adjusted to approximately pH = 3 using 8 mol L⁻¹ NaOH.

All prepared mixtures were placed in 23 mL Teflon-lined containers (Parr 4749). The hydrothermal treatment conditions were set to $t = 7$ days and $T = 250$ °C, under autogenous pressure. Final cooling to room temperature was carried out within one hour. The precipitates were then separated from the supernatants by centrifugation at 12 000 rpm for 12 min, washed twice with deionised water and once with ethanol, and finally dried overnight in an oven at 60 °C.

2.1.2. Purification procedure. Since most of the (Zr,U)SiO₄ syntheses resulted in a mixture of silicate and oxide, we further purified the zircon-type phase from the oxide phase based on the procedures already carried out for coffinite,⁴⁹ USiO₄, and uranothorite,⁸⁶ (U,Th)SiO₄. Dissolution of UO_{2+x} and/or (Zr,U)O_{2+x} was achieved by washing the synthesized mixtures with nitric acid, resulting in uranium oxidation. To



limit the dissolution of the silicate phase, the dissolution conditions were adapted to the mixture under consideration, using a stepwise approach that progressively acidified the media at each dissolution cycle and characterised the samples at each stage. This led to the selection of $[\text{HNO}_3] = 0.1 \text{ mol L}^{-1}$ for washing at 70 °C for 24 hours in the case of $(\text{Zr,U})\text{SiO}_4$ with $\text{U}/(\text{Zr} + \text{U}) = 60 \text{ mol}\%$, $[\text{HNO}_3] = 0.25 \text{ mol L}^{-1}$ for washing at 70 °C for 24 hours in the case of $(\text{Zr,U})\text{SiO}_4$ with $\text{U}/(\text{Zr} + \text{U}) = 50 \text{ mol}\%$, and $[\text{HNO}_3] = 1 \text{ mol L}^{-1}$ for washing at 70 °C for 24 hours in the case of $(\text{Zr,U})\text{SiO}_4$ with $\text{U}/(\text{Zr} + \text{U}) \leq 40 \text{ mol}\%$. 40 mg of the sample was added to 2 mL of the selected media and kept at 70 °C for one day under agitation on an IKA VXR Basic Vibrax shaker (2000 rpm) equipped with a heating device. The samples were then washed twice with water and once with ethanol and dried overnight in an oven at 60 °C.

2.2. Characterisation of the prepared samples

PXRD data were collected using a Bruker D8 Advance diffractometer equipped with a LynxEye detector and using $\text{Cu K}\alpha$ radiation ($\lambda = 1.54184 \text{ \AA}$) in reflection geometry (parallel beam) mode. Patterns were recorded between 5° and 90° (2θ) with 0.019° steps and a total counting time of 2.5 to 3 hours per sample. Pure silicon was used as the standard material to extract the instrumental function. The collected data were refined by the Rietveld method using the Fullprof suite package.⁸⁷ During refinement, various profiles and structural parameters were allowed to vary, such as zero shift, unit cell parameters, scale factor, and total displacement factor. However, the occupancy of each site was fixed to the calculated values.

Raman spectra were recorded using a Horiba-Jobin Yvon Aramis instrument equipped with an edge filter and a Nd:YAG laser (532 nm) delivering a 60 mW beam at the sample surface. The laser beam was then focused onto the sample using an Olympus BX 41 microscope with a $\times 50\text{LMP}$ objective, resulting in a spot area of $\sim 1 \mu\text{m}^2$. For each spectrum, the measurements were performed in the 100–1600 cm^{-1} range with a dwell time of 300 s. Three scans were recorded for each analysed area to minimise instrumental error. Fourier transform infrared (FTIR) spectra were recorded with a PerkinElmer FTIR Spectrum 100 instrument in the range of 550–4000 cm^{-1} . Powdered samples were deposited on the surface of an ATR crystal without prior preparation. Spectra collected under these operating conditions had a resolution of less than 4 cm^{-1} . Five scans were conducted for each sample to average the instrumental error.

Scanning electron microscopy (SEM) observations, implemented with energy dispersive X-ray spectroscopy (EDS), were made using an FEI Quanta 200 electronic microscope on small powder samples without any prior preparation. The electron microscope was equipped with either an Everhart-Thornley detector (ETD) or a back-scattered electron detector (BSED) under high vacuum conditions with a low accelerating voltage (2 kV). These conditions were chosen to produce a beam deceleration effect that allowed the acquisition of high-resolution images. Analyses by EDS coupled with SEM (Bruker

XFlash® 5010 SDD detector) were carried out on samples deposited directly onto an aluminium support. Elemental distribution maps and semi-quantitative determination of phase compositions were recorded at 15 kV, without any supplementary preparation. The particles observed were isolated from each other, and their size was small enough for no charging effect to occur.

Image analysis was performed using ImageJ/Fiji software.⁸⁸ To facilitate the segmentation of objects of interest, SEM images were optimized for high contrast between the background and particles. A Gaussian blur filter was applied to reduce high-frequency noise and improve the signal-to-noise ratio. Counting and morphological analyses were performed semi-automatically. Isolated and agglomerated particles were segmented, counted and analysed automatically and manually, respectively.

Thermogravimetric analysis (TGA) was performed to determine the hydration content of the samples prepared at the end of the syntheses and the thermal stability of the $(\text{Zr,U})\text{SiO}_4$ solid solutions. All these analyses were performed between room temperature and 1000 °C at a heating rate of 5 °C min^{-1} under an argon atmosphere using a SETSYS evolution TG/DTG analyser.

3. Results and discussion

3.1. Hydrothermal synthesis of $(\text{Zr,U})\text{SiO}_4$ with different uranium contents

Attempts were made to synthesise $(\text{Zr,U})\text{SiO}_4$ solid solutions based on the conditions identified in previous work for the synthesis of ZrSiO_4 .⁸³ Since 7 days of hydrothermal treatment at 250 °C were found to be sufficient to prepare synthetic zircon with a concentration of reactants (silicate and $\text{Zr} + \text{U}$) of 0.2 mol L^{-1} , these conditions were chosen as the reference for the study of $(\text{Zr,U})\text{SiO}_4$ solid solutions. In an effort to promote Zr substitution by U in the ZrSiO_4 lattice, the acidity of the reactive media was chosen to be $\text{pH} = 3$. On the one hand, these conditions allow favourable interactions between the silicate ($\text{Si}(\text{OH})_4$) and the tetravalent metal ions according to the work of Iler⁸⁵ and to promote the nucleation of metal silicate phases. On the other hand, these conditions appeared to be a compromise to limit the formation of large amounts of oxide as a secondary phase, which could be expected at higher pH values. The zirconium and uranium reactants were in the +4 oxidation state and all experiments were carried out in hydrochloric acid reactive media to limit the $\text{U}(\text{IV})$ oxidation to $\text{U}(\text{VI})$. All experiments were carried out under an air atmosphere.

The syntheses were carried out with $\text{U}/(\text{Zr} + \text{U})$ molar fractions ranging from 0 to 90 mol% (*i.e.* Zr:U molar ratios ranging from 100:0 to 10:90). The results of the PXRD analyses showed the formation of a zircon-type silicate phase from up to 60 mol% (Fig. 1), with the presence of XRD lines corresponding to the tetragonal $I4_1/amd$ structure. A progressive shift towards lower angles was observed with increasing uranium content, corresponding to uranium incorporation



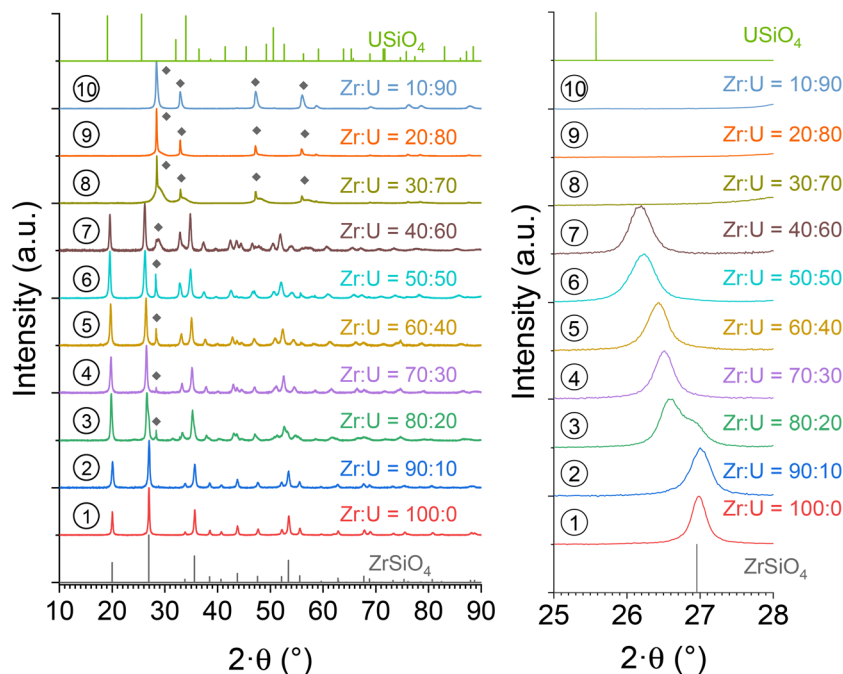


Fig. 1 PXRD patterns recorded for pristine $(\text{Zr,U})\text{SiO}_4$ solid solutions of different chemical compositions prepared under hydrothermal conditions without purification ($T = 250\text{ }^\circ\text{C}$, 7 days, $\text{pH} = 3.0$) from Zr + U and silicate concentrations of 0.2 mol L^{-1} for Zr : U = 100 : 0 (1), 90 : 10 (2), 80 : 20 (3), 70 : 30 (4), 60 : 40 (5), 50 : 50 (6), 40 : 60 (7), 30 : 70 (8), 20 : 80 (9) and 10 : 90 (10). The presence of $(\text{Zr,U})\text{O}_{2+x}$ (fluorite-type) is indicated by diamond symbols in the PXRD patterns. The Bragg positions of the characteristic peaks of ZrSiO_4 and USiO_4 have been extracted from ref. 89 and 90, respectively.

into the ZrSiO_4 lattice. Above 20 mol% uranium content, the hydrothermal syntheses resulted in multiple phases with the formation of secondary oxide phases. Well-crystallised cubic UO_{2+x} (space group $Fm\bar{3}m$) and poorly crystallized nanometric cubic $(\text{Zr,U})\text{O}_{2+x}$ (space group $Fm\bar{3}m$) were simultaneously obtained. For uranium contents above 70 mol%, the silicate phase was no longer obtained, resulting only in the formation of a mixture of cubic UO_{2+x} and cubic $(\text{Zr,U})\text{O}_{2+x}$.

Rietveld refinements were performed on all pristine (prior to any purification or annealing) solid solutions. Irrespective of the potential hydration rate of the zircon-type phases, the $(\text{Zr,U})\text{SiO}_4$ unit cell parameters were found to approximately follow Vegard's (regarding linear variation over the lattice parameters) and Retger's (regarding pseudo-linear volume variation over the lattice volume) laws that assume a close-to-ideal solid solution (Fig. 2 and Table SI 2†). This result is in very good agreement with progressive substitution of zirconium by uranium in the zircon-type structure with maximum insertion molar ratios of up to 50–60 mol%, which are far above the maximum insertion rates reported in the literature (*i.e.* 25 mol% (ref. 82)). This also demonstrates that, despite the thermodynamic instability of these compounds,⁷¹ the $(\text{Zr,U})\text{SiO}_4$ solid solution exhibits close-to-ideal solubility behaviour from a structural point of view.

Rietveld refinements were carried out on the secondary oxide phases (Fig. SI 1 and Table SI 3†). This allowed the identification of the two phases to be confirmed:

- The first phase, fairly well-crystallised, obtained for $\text{U}/(\text{Zr} + \text{U})$ molar fractions ranging from 20 to 90 mol%, corresponding to UO_{2+x} (or to $(\text{U,Zr})\text{O}_{2+x}$ with a very small amount of zirconium inserted in the UO_2 lattice).

- The second phase, poorly crystallised or nanometric, was obtained for a $\text{U}/(\text{Zr} + \text{U})$ molar fraction between 50 and 90 mol%, corresponding to $(\text{Zr,U})\text{O}_{2+x}$. The zirconium insertion in the UO_2 lattice could be estimated to correspond to a $\text{Zr}/(\text{Zr} + \text{U})$ molar fraction as high as 25–30 mol%.

From an experimental point of view, the formation of the $(\text{Zr,U})\text{O}_{2+x}$ phase could correspond to a kinetically formed by-product due to the difficulty of obtaining the $(\text{Zr,U})\text{SiO}_4$ species under the experimental conditions considered. On the other hand, the UO_{2+x} phases could originate from a dissolution and reprecipitation process involving $(\text{Zr,U})\text{SiO}_4$ or $(\text{Zr,U})\text{O}_{2+x}$ species and as a thermodynamic product under the synthesis conditions. This interpretation could be supported by the fact that the observed $(\text{Zr,U})\text{SiO}_4$ and $(\text{Zr,U})\text{O}_{2+x}$ species have $\text{U}/(\text{Zr} + \text{U})$ molar ratios very close to the experimentally expected values.

Infrared spectroscopy characterisation was performed for all samples (Fig. 3), and the characteristic features of SiO_4 modes were observed in the spectra for molar fraction $\text{U}/(\text{Zr} + \text{U})$ values, ranging from 0 to 60 mol%, allowing the formation of the $(\text{Zr,U})\text{SiO}_4$ phase to be confirmed under these conditions. The symmetric ν_1 and antisymmetric ν_3 stretching modes were located close to $860\text{--}850\text{ cm}^{-1}$ and



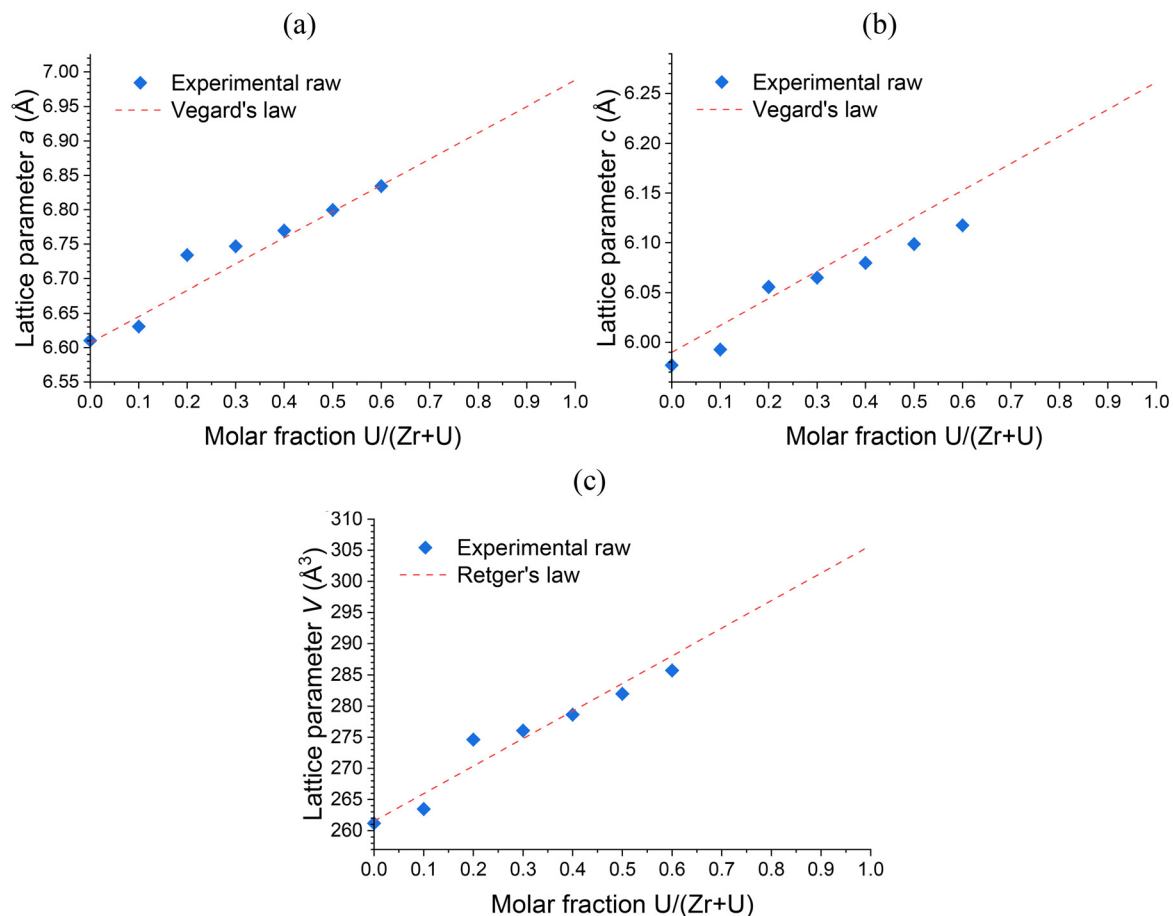


Fig. 2 Unit cell parameters a (a) and c (b) and volume V (c) of the zircon-type phase obtained by Rietveld refinements performed on PXRD patterns of pristine $(\text{Zr,U})\text{SiO}_4$ solid solutions prepared under hydrothermal conditions without purification ($T = 250\text{ }^\circ\text{C}$, 7 days, $\text{pH} = 3.0$) starting with $\text{Zr} + \text{U}$ and silicate concentrations of 0.2 mol L^{-1} with different chemical compositions. Reference lattice parameters for the Vegard's and the Retger's laws have been obtained from ref. 70 and 74.

$1050\text{--}980\text{ cm}^{-1}$, respectively. The antisymmetric bending mode ν_4 was identified around $620\text{--}590\text{ cm}^{-1}$ and the symmetric bending mode ν_2 at around 430 cm^{-1} . In addition, the antisymmetric and symmetric bending modes of SiO_2 were clearly observed at 1070 and 800 cm^{-1} , respectively, for the samples with $\text{U}/(\text{Zr} + \text{U})$ molar fractions above 60 mol%.

As the ν_4 vibrational mode shows significant variation and is easily identifiable in infrared spectroscopy (Fig. 4), it could be used to assess the incorporation rate of U into $(\text{Zr,U})\text{SiO}_4$. Comparison with the ν_4 band position for a reference USiO_4 sample ($\nu_4 = 569\text{ cm}^{-1}$) and reported in the literature for ZrSiO_4 ($\nu_4 = 620\text{ cm}^{-1}$)⁹¹ allows a linear relationship of the band position with the molar fraction $\text{U}/(\text{Zr} + \text{U})$ from 0 to 60 mol% (Fig. 4 and Fig. SI 2†). These results support the hypothesis of a progressive substitution of zirconium by uranium in the zircon-type structure with a maximum inserted molar fraction of up to 50–60 mol%.

In addition, the infrared spectra allowed the presence of residual water and/or hydroxyl groups in the pristine samples to be observed through the observation of associated weak bands in the $3700\text{--}2800\text{ cm}^{-1}$ region, with either being indi-

cated by the water bending mode at 1638 cm^{-1} (Fig. 3), as was previously observed for ZrSiO_4 , CeSiO_4 , and USiO_4 .^{83,92}

Raman characterisation was carried out on the samples showing the presence of the $(\text{Zr,U})\text{SiO}_4$ phase (Fig. 5). It allows the features of the SiO_4 modes to be observed, with the symmetric ν_1 and antisymmetric ν_3 stretching modes located at $970\text{--}900\text{ cm}^{-1}$ and $1010\text{--}960\text{ cm}^{-1}$, respectively, and the ν_2 symmetric bending mode around $440\text{--}420\text{ cm}^{-1}$. However, the ν_3 mode was difficult to identify as this weak band is masked by the intense ν_1 band. The ν_4 antisymmetric mode is located close to 610 cm^{-1} but was difficult to observe due to its very low intensity. In addition, the internal modes of zircon silicate (below 400 cm^{-1}) were also observed. Apart from these bands, a signal of very variable intensity was observed around 700 cm^{-1} , as reported by Clavier *et al.*⁹³ This band could be correlated to the optical emission of $\text{U}(\text{IV})$ in the zircon-type matrix with the laser radiation used (Nd:YAG at 532 nm).

In addition, since the position of the ν_1 band can be easily determined and shows a strong variation from ZrSiO_4 to USiO_4 , these positions were compared for all samples and allowed a linear relationship of the band position with the



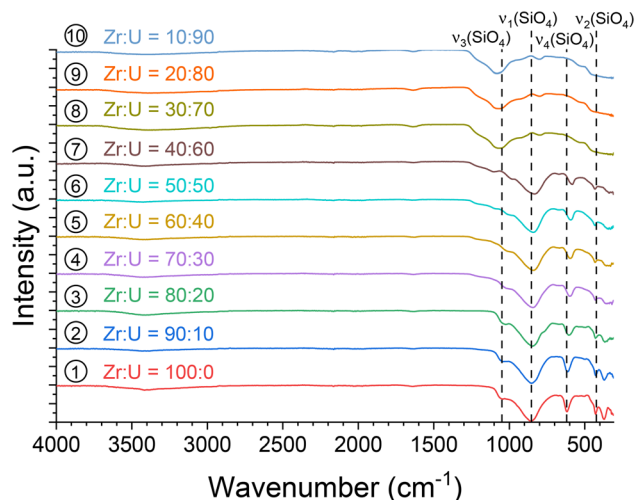


Fig. 3 Infrared spectra recorded for pristine $(\text{Zr,U})\text{SiO}_4$ solid solutions of different chemical compositions prepared under hydrothermal conditions without purification ($T = 250\text{ }^\circ\text{C}$, 7 days, $\text{pH} = 3.0$) from Zr + U and silicate concentrations of 0.2 mol L^{-1} for Zr : U = 100 : 0 (1), 90 : 10 (2), 80 : 20 (3), 70 : 30 (4), 60 : 40 (5), 50 : 50 (6), 40 : 60 (7), 30 : 70 (8), 20 : 80 (9) and 10 : 90 (10). The positions of the characteristic bands of the silicate group have been given for ZrSiO_4 .

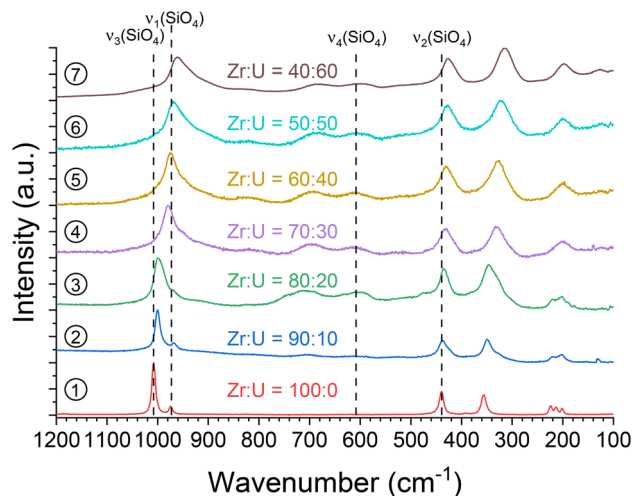


Fig. 5 Raman spectra recorded for pristine $(\text{Zr,U})\text{SiO}_4$ solid solutions with different chemical compositions prepared under hydrothermal conditions without purification ($T = 250\text{ }^\circ\text{C}$, 7 days, $\text{pH} = 3.0$) starting with Zr + U and silicate concentrations of 0.2 mol L^{-1} for Zr : U = 100 : 0 (1), 90 : 10 (2), 80 : 20 (3), 70 : 30 (4), 60 : 40 (5), 50 : 50 (6) and 40 : 60 (7). The positions of the characteristic bands of the silicate group have been given for ZrSiO_4 . They are indicated by the broken lines.

molar fraction $\text{U}/(\text{Zr} + \text{U})$ varying from 0 to 60 mol% to be observed (Fig. 6 and Fig. SI 3[†]). A similar behaviour was also observed for the position of the ν_2 band (Fig. SI 4 and SI 5[†]). All these results support the hypothesis of uranium incorporation into the zircon structure.

In order to obtain information on the morphology resulting from the synthesis, $\text{Zr}_{0.8}\text{U}_{0.2}\text{SiO}_4$ (3), $\text{Zr}_{0.6}\text{U}_{0.4}\text{SiO}_4$ (5) and

$\text{Zr}_{0.4}\text{U}_{0.6}\text{SiO}_4$ (7) pristine samples were observed by SEM (Fig. 7). It can be seen that the sample is composed of sub-micron particles (Fig. 7), with the samples doped with 20 mol% and 40 mol% uranium having a particle size below 100 nm with a fairly homogeneous size distribution (Fig. 7a and b). These particles have an angular shape, which may correspond to the characteristic square-based bipyramidal

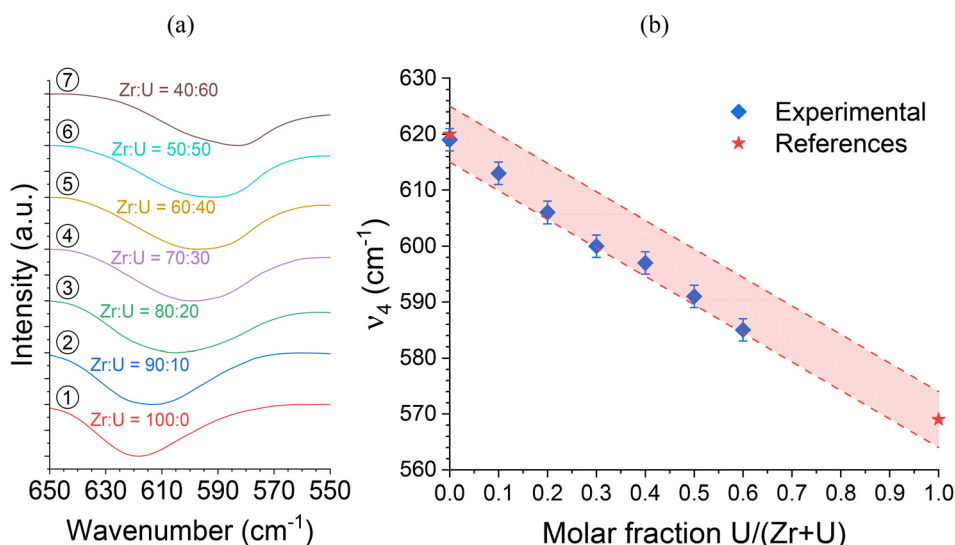


Fig. 4 (a) Infrared spectra of the SiO_4 group ν_4 band recorded for pristine $(\text{Zr,U})\text{SiO}_4$ solid solutions with different chemical compositions prepared under hydrothermal conditions without purification ($T = 250\text{ }^\circ\text{C}$, 7 days, $\text{pH} = 3.0$) from Zr + U and silicate concentrations of 0.2 mol L^{-1} for Zr : U = 100 : 0 (1), 90 : 10 (2), 80 : 20 (3), 70 : 30 (4), 60 : 40 (5), 50 : 50 (6), 40 : 60 (7), 30 : 70 (8), 20 : 80 (9) and 10 : 90 (10). (b) Position of the ν_4 band as a function of the expected $\text{U}/(\text{Zr} + \text{U})$ molar fraction. The reference ZrSiO_4 ν_4 band position has been taken from ref. 91. The shaded area corresponds to the expected linear variation of the ν_4 band of the SiO_4 group in IR spectroscopy, based on reference values reported in the literature, with a confidence interval of 5 cm^{-1} .



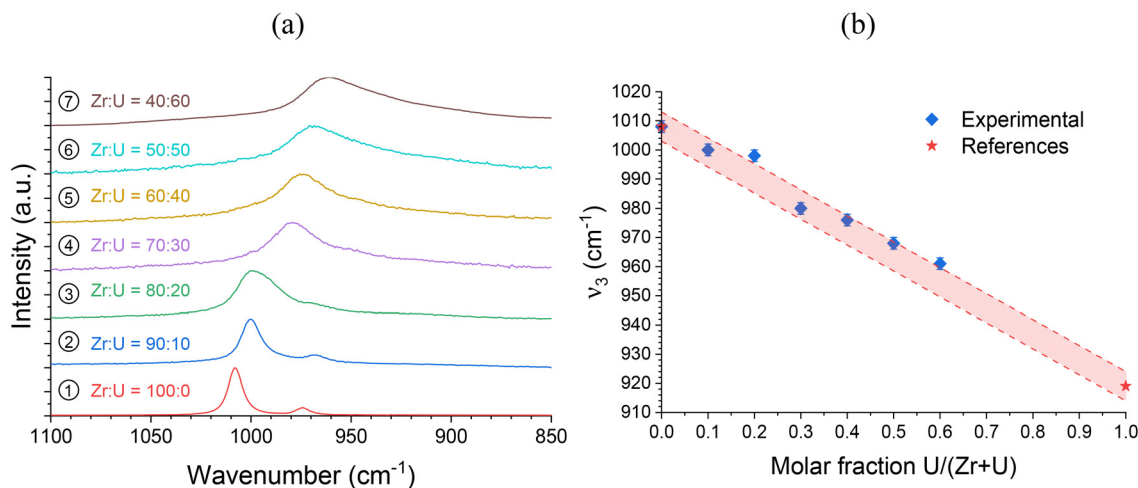


Fig. 6 (a) Raman spectra of the SiO_4 group ν_3 band recorded for pristine $(\text{Zr,U})\text{SiO}_4$ solid solutions of different chemical compositions prepared under hydrothermal conditions without purification ($T = 250\text{ }^\circ\text{C}$, 7 days, $\text{pH} = 3.0$) starting with Zr + U and silicate concentrations of 0.2 mol L^{-1} for Zr : U = 100 : 0 (1), 90 : 10 (2), 80 : 20 (3), 70 : 30 (4), 60 : 40 (5), 50 : 50 (6) and 40 : 60 (7). (b) Position of the ν_3 band as a function of the expected U/(Zr + U) molar fraction. Reference ν_3 band positions for ZrSiO_4 and USiO_4 have been taken from ref. 93. The shaded area corresponds to the expected linear variation of the ν_3 band of the SiO_4 group in Raman spectroscopy, based on reference values reported in the literature, with a confidence interval of 5 cm^{-1} .

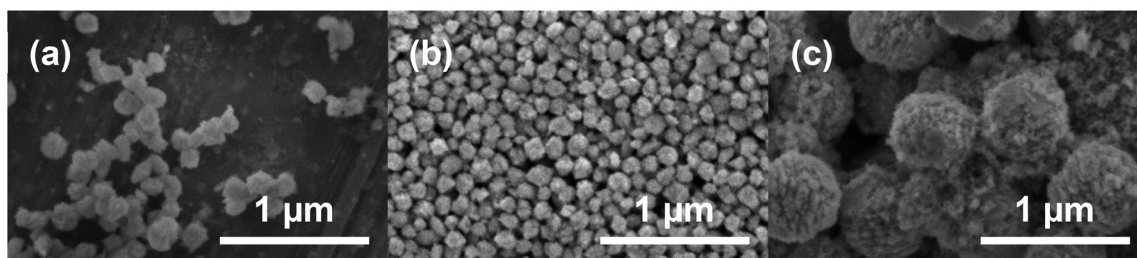


Fig. 7 SEM micrographs of pristine $(\text{Zr,U})\text{SiO}_4$ solid solutions prepared under hydrothermal conditions ($T = 250\text{ }^\circ\text{C}$, 7 days, $\text{pH} = 3.0$) starting from Zr + U and silicate concentrations of 0.2 mol L^{-1} for Zr : U = 80 : 20 (3) (a), 60 : 40 (5) (b) and 40 : 60 (7) (c).

morphology of the silicate group compounds, although the very small particle size makes it difficult to confirm this result. On the other hand, the sample doped with 60 mol% uranium shows a spheroidal morphology with polycrystalline particles of about 500 nm (Fig. 7c). In addition, a halo, probably related to the presence of nanometric particles of uranium and zirconium–uranium oxides, can be observed for the 40 mol% and 60 mol% samples (Fig. 7b and c).

3.2. Purification procedure

In order to purify the samples from the secondary oxide phases, a dissolution procedure was developed based on that used for USiO_4 and $(\text{Th,U})\text{SiO}_4$ solid solutions.^{49,86} All samples containing $(\text{Zr,U})\text{SiO}_4$ were washed by oxidative dissolution in weakly concentrated nitric acid reactive media using a gradual approach, depending on the chemical composition of the sample. This led to the selection of $[\text{HNO}_3] = 0.1\text{ mol L}^{-1}$, $[\text{HNO}_3] = 0.25\text{ mol L}^{-1}$ and $[\text{HNO}_3] = 1\text{ mol L}^{-1}$ washing media for $\text{Zr}_{0.4}\text{U}_{0.6}\text{SiO}_4$, $\text{Zr}_{0.5}\text{U}_{0.5}\text{SiO}_4$ and $\text{Zr}_{1-x}\text{U}_x\text{SiO}_4$ ($x \leq 0.40$),

respectively. The washing process was stopped when the oxide phase was below the detection limit. This procedure allowed the dissolution of the oxide phases with fairly good selectivity, resulting in pure $(\text{Zr,U})\text{SiO}_4$ samples (Fig. 8). The unit cell parameters of the purified $(\text{Zr,U})\text{SiO}_4$ phases were determined again by the Rietveld refinement method (Table SI 2†) and showed no significant differences with respect to previously measured parameters. Infrared spectroscopic characterisation also showed no significant differences (Fig. SI 6† and Fig. 14).

In order to evaluate the effect of nitric acid washing on the morphology of the silicate phase, complementary SEM observations were carried out on the purified samples (Fig. 9). It was observed that there was no particular alteration feature or morphology changes on the largest particles compared to that observed in SEM on the pristine samples (Fig. 7). However, this seems difficult to confirm with certainty, given both the very small size of the particles observed and the magnification used in the observation. Nevertheless, the smallest particles previously observed on the uranium and zirconium–uranium



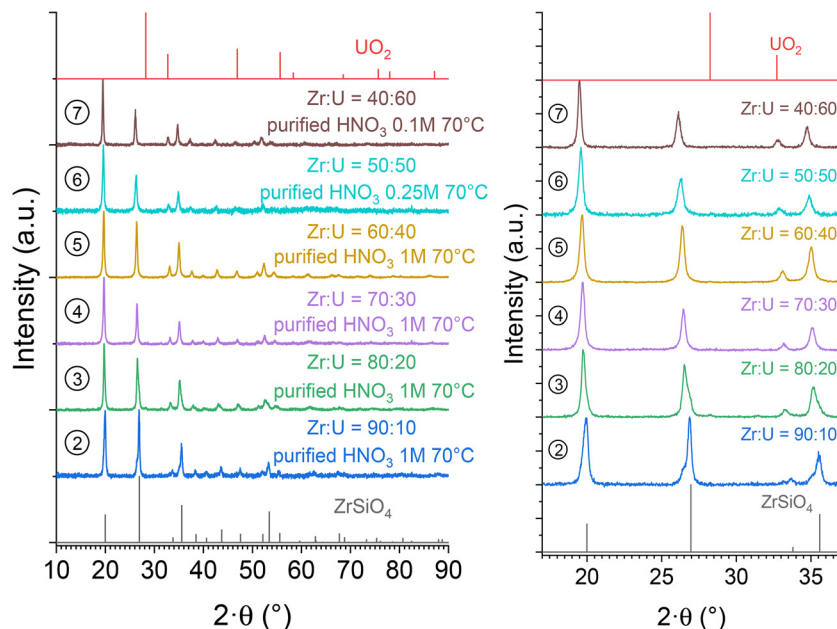


Fig. 8 PXRD patterns recorded for purified $(\text{Zr,U})\text{SiO}_4$ solid solutions of different chemical compositions prepared under hydrothermal conditions ($T = 250^\circ\text{C}$, 7 days, $\text{pH} = 3.0$) starting with Zr + U and silicate concentrations of 0.2 mol L^{-1} for Zr : U = 90 : 10 (2), 80 : 20 (3), 70 : 30 (4), 60 : 40 (5), 50 : 50 (6), and 40 : 60 (7), and washed in nitric acid media. Bragg positions of the characteristic peaks of ZrSiO_4 and UO_2 have been extracted from ref. 89 and 94, respectively.

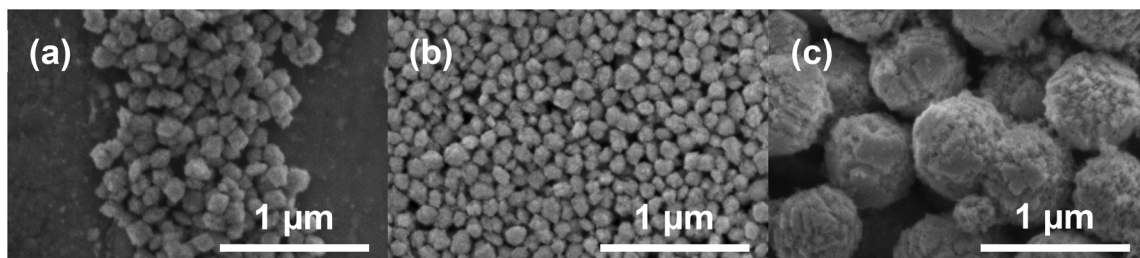


Fig. 9 SEM micrographs of purified $(\text{Zr,U})\text{SiO}_4$ solid solutions prepared under hydrothermal conditions ($T = 250^\circ\text{C}$, 7 days, $\text{pH} = 3.0$) starting with Zr + U and silicate concentrations of 0.2 mol L^{-1} for Zr : U = 80 : 20 (3) (a), 60 : 40 (5) (b) and 40 : 60 (7) (c) and washed in nitric acid media. Observations at different magnifications are available in Fig. SI 7.†

oxide samples (and attributed to the oxide phases) were no longer observed in the purified samples, in agreement with the PXRD results.

Elemental mapping was also carried out on the $\text{Zr}_{0.4}\text{U}_{0.6}\text{SiO}_4$ sample (Fig. 10) using EDS. These measurements confirmed that the particles observed correspond to the zircon-type silicate phase and that zirconium and uranium are homogeneously distributed throughout the sample. EDS quantification performed on $\text{Zr}_{0.8}\text{U}_{0.2}\text{SiO}_4$, $\text{Zr}_{0.6}\text{U}_{0.4}\text{SiO}_4$ and $\text{Zr}_{0.4}\text{U}_{0.6}\text{SiO}_4$ samples gave experimental molar ratios $\text{U}/(\text{Zr} + \text{U})$ of $29 \pm 8\text{ mol}\%$, $47 \pm 13\text{ mol}\%$ and $60 \pm 4\text{ mol}\%$, respectively. These results reflect the increase in uranium content in the sample. The experimental values are in the right order of magnitude (considering the uncertainties) but may vary significantly from the target values. These results and the associated uncertainties could be explained with synthesis para-

meters but they also reflect the limitations of such semi-quantitative analysis on nanometric samples. On the other hand, the EDS data treatment may also lead to an underestimation of the amount of uranium compared to zirconium.

In addition, the particle size distribution was verified from SEM observations in the BSE (back scattering electron) mode and data treatment (based on 1734 identified particles) by computer processing using ImageJ/Fiji software. This confirmed that the $(\text{Zr,U})\text{SiO}_4$ sample has a relatively homogeneous particle size distribution with a mean size (volume ponderation) of 310 nm (Fig. 11).

3.3. Annealing of $(\text{Zr,U})\text{SiO}_4$

In order to assess the presence of water/hydroxyl groups in these compounds and to obtain anhydrous samples, the purified $(\text{Zr,U})\text{SiO}_4$ samples were characterised by TGA under an



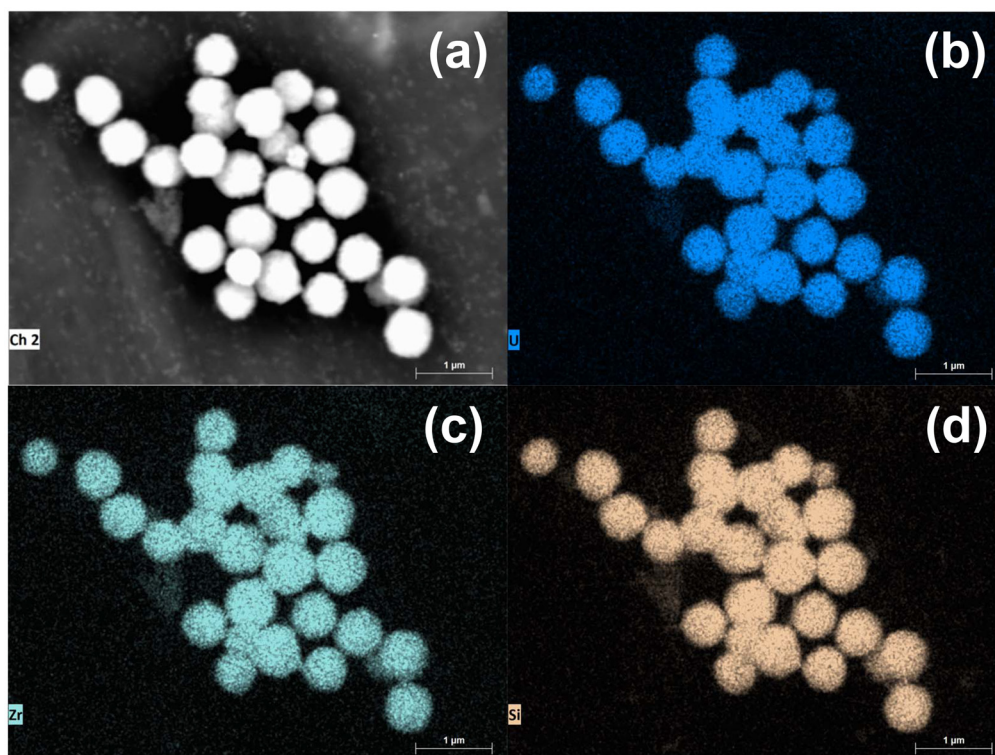


Fig. 10 SEM micrographs in BSE mode (a) of purified $(\text{Zr,U})\text{SiO}_4$ solid solution prepared under hydrothermal conditions ($T = 250\text{ }^\circ\text{C}$, 7 days, $\text{pH} = 3.0$) starting with Zr + U and silicate concentrations of 0.2 mol L^{-1} for Zr : U = 40 : 60 (7) washed in 0.1 mol L^{-1} nitric acid media. Corresponding EDS maps for uranium (b), zirconium (c) and silicon (d).

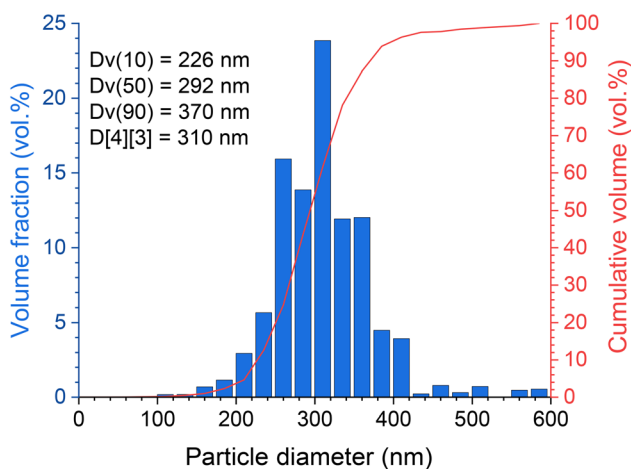


Fig. 11 Particle size distribution, based on SEM observation data treatment with volume ponderation, for purified $(\text{Zr,U})\text{SiO}_4$ solid solution prepared under hydrothermal conditions ($T = 250\text{ }^\circ\text{C}$, 7 days, $\text{pH} = 3.0$) starting with Zr + U and silicate concentrations of 0.2 mol L^{-1} for Zr : U = 40 : 60 (7) washed in 0.1 mol L^{-1} nitric acid media.

argon atmosphere up to $1000\text{ }^\circ\text{C}$ (Fig. SI 8[†]). The argon atmosphere was chosen to prevent uranium(IV) oxidation, which could occur under an air atmosphere at high temperature. These analyses show that the dehydration/dehydroxylation process occurred in several steps for temperatures up to

$700\text{--}800\text{ }^\circ\text{C}$ for all samples with the water/hydroxo content corresponding to 2–3% of the initial sample mass. This progressive mass loss is in agreement with the previous studies

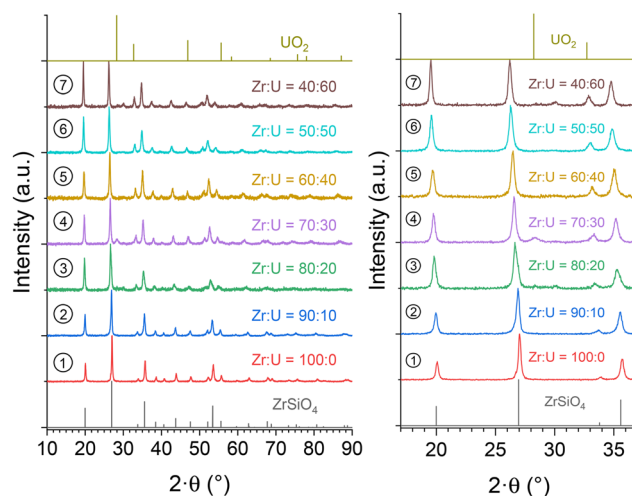


Fig. 12 PXRD patterns recorded for purified $(\text{Zr,U})\text{SiO}_4$ solid solutions calcined at $1200\text{ }^\circ\text{C}$ under an Ar-H_2 atmosphere with different chemical compositions prepared under hydrothermal conditions ($T = 250\text{ }^\circ\text{C}$, 7 days, $\text{pH} = 3.0$) starting with Zr + U and silicate concentrations of 0.2 mol L^{-1} for Zr : U = 90 : 10 (2), 80 : 20 (3), 70 : 30 (4), 60 : 40 (5), 50 : 50 (6), and 40 : 60 (7). The Bragg positions of the characteristic peaks of ZrSiO_4 and UO_2 have been taken from ref. 89 and 94, respectively.



which identified high-temperature water losses for the zircon-type systems due to the water/hydroxo content trapped in the [001] channels of the silicate phase.⁹² The presence of hydroxyl species has also been identified for USiO_4 and is likely to occur for $(\text{Zr,U})\text{SiO}_4$ systems. Furthermore, it appears that the weight loss is negatively correlated with the expected uranium incorporation content.

The thermally treated TGA residues were characterised by PXRD analyses; these analyses confirmed that the zircon-type phase was preserved under these conditions, both from uranium oxidation and from the degradation of the silicate structure to an oxide mixture (Fig. SI 9†). In order to obtain more information on the thermal stability of these phases at higher temperatures, $(\text{Zr,U})\text{SiO}_4$ samples were heated at 1200 °C under an argon–hydrogen atmosphere ($\text{Ar} + \text{H}_2$ 4%) with an isothermal step of 1 hour at the target temperature. No strong evidence of decomposition of the silicate phase into SiO_2 and $(\text{Zr,U})\text{O}_2$ was observed from PXRD (Fig. 12), the presence of $(\text{Zr,U})\text{O}_2$ oxide as a minor phase for $\text{Zr}_{0.7}\text{U}_{0.3}\text{SiO}_4$ being attributed to residual oxide remaining after an insufficient purification step.

Furthermore, Rietveld refinements carried out on heated samples showed a decrease in the unit cell parameter, which is characteristic of dehydration/dehydroxylation of zircon-type samples, but the data remained consistent with the results of uranium insertion into the ZrSiO_4 structure. The uranium content in the $(\text{Zr,U})\text{SiO}_4$ solid solution does not seem to be significantly affected by the purification process or by heating treatment up to 1200 °C (Fig. 13).

In addition, the samples calcinated at 1200 °C were characterised using vibrational spectroscopy techniques. Both infrared (Fig. 14) and Raman (Fig. 15) spectra were in agreement with the results of PXRD. Both sets of spectra show the characteristic bands of the silicate groups in the $(\text{Zr,U})\text{SiO}_4$ structure without any significant shift with respect to the position determined for the pristine samples (which could have indicated changes in the phase composition) (Fig. SI 10–SI 12†). Furthermore, the characteristic T_{2g} band of the cubic uranium oxide is not observed in the Raman spectra, suggesting an amount below the detection limit of potential oxide phases. Finally, the infrared spectra show dehydration/dehydroxylation of the samples as the characteristic bands of water/hydroxyl

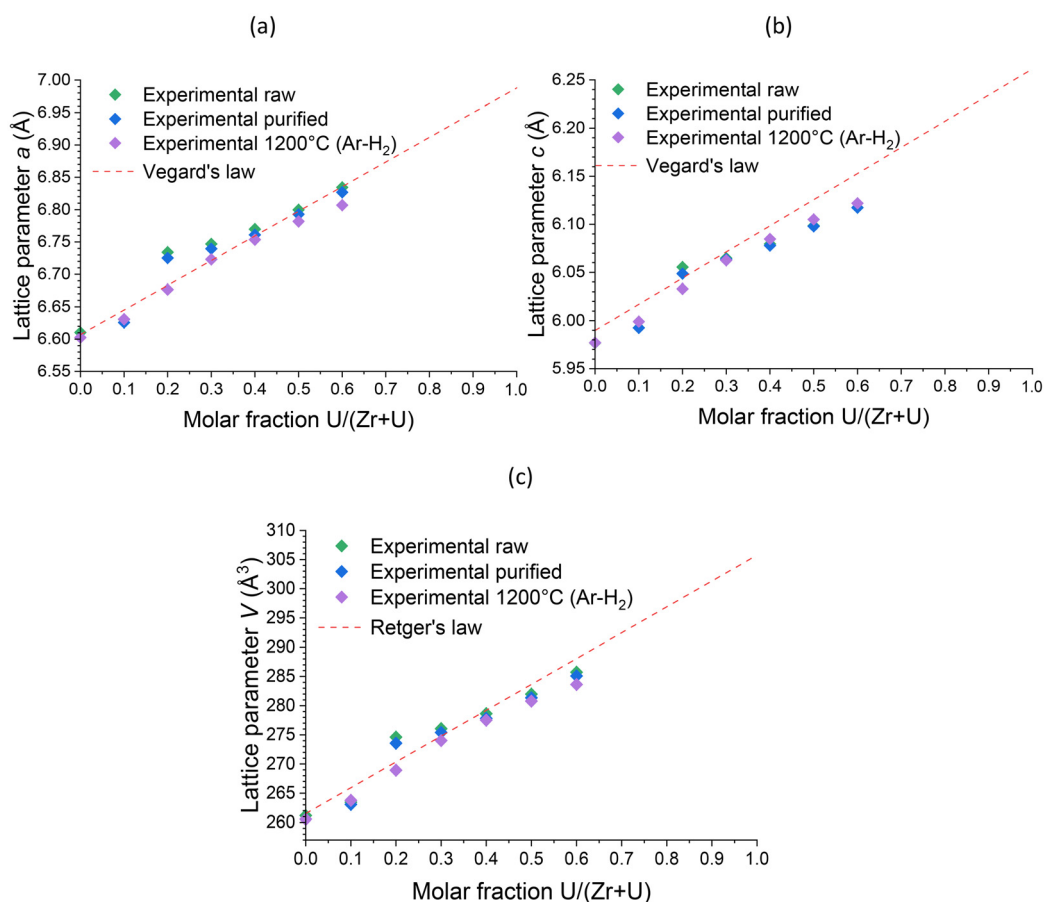


Fig. 13 Unit cell parameters a (a) and c (b) and volume V (c) of the zircon-type phase obtained by Rietveld refinements performed on PXRD patterns of pristine, purified and calcined at 1200 °C $(\text{Zr,U})\text{SiO}_4$ solid solutions prepared under hydrothermal conditions ($T = 250$ °C, 7 days, $\text{pH} = 3.0$) starting with $\text{Zr} + \text{U}$ and silicate concentrations of 0.2 mol L^{-1} with different chemical compositions. Reference lattice parameters for Vegard's and the Retger's laws have been obtained from ref. 70 and 74.



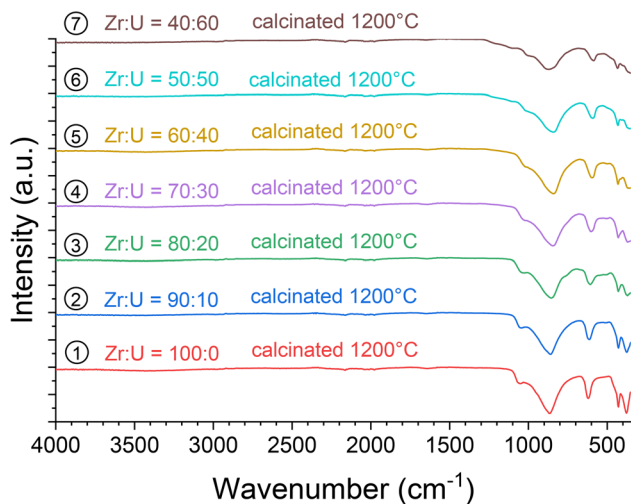


Fig. 14 Infrared spectra recorded for purified $(\text{Zr,U})\text{SiO}_4$ solid solutions then calcinated at 1200 °C under an Ar-H_2 atmosphere with different chemical compositions prepared under hydrothermal conditions ($T = 250$ °C, 7 days, $\text{pH} = 3.0$) starting with $\text{Zr} + \text{U}$ and silicate concentrations of 0.2 mol L^{-1} for $\text{Zr} : \text{U} = 90 : 10$ (2), $80 : 20$ (3), $70 : 30$ (4), $60 : 40$ (5), $50 : 50$ (6), and $40 : 60$ (7).

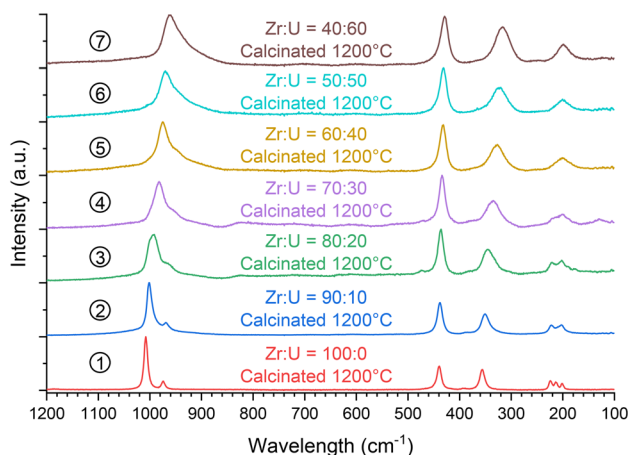


Fig. 15 Raman spectra recorded for purified $(\text{Zr,U})\text{SiO}_4$ solid solutions then calcinated at 1200 °C under an Ar-H_2 atmosphere with different chemical compositions prepared under hydrothermal conditions ($T = 250$ °C, 7 days, $\text{pH} = 3.0$) starting with $\text{Zr} + \text{U}$ and silicate concentrations of 0.2 mol L^{-1} for $\text{Zr} : \text{U} = 90 : 10$ (2), $80 : 20$ (3), $70 : 30$ (4), $60 : 40$ (5), $50 : 50$ (6), and $40 : 60$ (7).

groups (weak bands in the $3700\text{--}2800 \text{ cm}^{-1}$ region) are no longer observed.

4. Conclusion

Based on the results previously reported in the literature,⁸³ the synthesis of $(\text{Zr,U})\text{SiO}_4$ solid solutions was studied under soft hydrothermal conditions ($T = 250$ °C, 7 days holding time, $C_{\text{Zr+U}} = 0.2 \text{ mol L}^{-1}$, $\text{pH} = 3.0$). These conditions allowed the

formation of $(\text{Zr,U})\text{SiO}_4$ samples with uranium contents up to 60 mol%, well above the previously reported maximum insertion rate (*i.e.* 25 mol%)⁸² and the calculated thermodynamic stability limit for this solid solution.⁷¹ This result was confirmed by PXRD, infrared spectroscopy and Raman spectroscopy.

Furthermore, since the as-prepared samples contained secondary oxide phases, a purification procedure based on nitric acid washes was established, which allowed the preparation of oxide-free $(\text{Zr,U})\text{SiO}_4$ samples. These purified samples were then characterised by thermogravimetric analysis. On the one hand, it was observed that the total water content of the hydrothermally synthesised $(\text{Zr,U})\text{SiO}_4$ samples decreases with an increasing uranium insertion rate. On the other hand, it has been shown that uranium-rich zircon-type phases, with up to 60 mol% uranium, remain stable up to 1200 °C under a reducing atmosphere (Ar-H_2), allowing dehydrated samples to be obtained.

These results represent major steps forward in the study of $(\text{Zr,An})\text{SiO}_4$ solid solutions, which are known to form under accidental conditions, and will allow direct evaluation of the properties of these solid solutions. In this perspective, a complementary calorimetric study is underway to learn more about the thermodynamic parameters of $(\text{Zr,U})\text{SiO}_4$, such as enthalpy of formation and enthalpy of mixing.

Data availability

The data supporting this article have been included as part of the ESI.†

Conflicts of interest

The authors declare no competing financial interest.

Acknowledgements

The present work was supported by the EPIC project funded by the French NEEDS (Nucléaire: Energie, Environnement, Déchets, Société) program (CNRS, CEA, ANDRA, BRGM, EDF, FRAMATOME, IRSN, ORANO).

References

- 1 L. T. White and T. R. Ireland, *Chem. Geol.*, 2012, **306–307**, 78–91.
- 2 P. A. Nevolko, T. V. Svetlitskaya, A. A. Savichev, V. S. Vesnin and P. A. Fominykh, *Ore Geol. Rev.*, 2021, **139**, 104532.
- 3 R. C. Ewing, A. Meldrum, L. M. Wang, W. J. Weber and L. R. Corrales, *Rev. Mineral. Geochem.*, 2003, **53**, 388–425.
- 4 P. W. O. Hoskin and U. Schaltegger, *Rev. Mineral. Geochem.*, 2003, **53**, 27–62.



- 5 L. Nasdala, J. M. Hanchar, D. Rhed, A. K. Kennedy and T. Váczi, *Chem. Geol.*, 2010, **269**, 290–300.
- 6 K. Breiter, H. J. Förster and R. Skoda, *Lithos*, 2006, **88**, 15–34.
- 7 E. V. Shalaeva, A. M. Murzakaev, V. V. Makarov, V. G. Pushin, D. A. Zamyatin, Y. V. Shchapova and S. L. Votyakov, *Glass Phys. Chem.*, 2015, **41**, 389–397.
- 8 S. Moorbath, *Nature*, 1986, **321**, 725.
- 9 J. W. Valley, A. J. Cavosie, T. Ushikubo, D. A. Reinhard, D. F. Lawrence, D. J. Larson, P. H. Clifton, T. F. Kelly, S. A. Wilde, D. E. Moser and M. J. Spicuzza, *Nat. Geosci.*, 2014, **7**, 219–223.
- 10 D. O. Froude, T. R. Ireland, P. D. Kinny, I. S. Williams, W. Compston, I. R. Williams and J. S. Myers, *Nature*, 1983, **304**, 616–618.
- 11 R. Maas, P. D. Kinny, I. S. Williams, D. O. Froude and W. Compston, *Geochim. Cosmochim. Acta*, 1992, **56**, 1281–1300.
- 12 W. J. Weber, *J. Am. Ceram. Soc.*, 1993, **76**, 1729–1738.
- 13 T. Murakami, B. C. Chakoumakos, R. C. Ewing, G. R. Lumpkin and W. J. Weber, *Am. Mineral.*, 1991, **76**, 1510–1532.
- 14 W. J. Weber, R. C. Ewing and L. M. Wang, *J. Mater. Res.*, 1994, **9**, 688–698.
- 15 H. D. Holland and D. Gottfried, *Acta Crystallogr.*, 1955, **8**, 291–300.
- 16 S. Rios, E. K. H. Salje, M. Zhang and R. C. Ewing, *J. Phys.: Condens. Matter*, 2000, **12**, 2401–2412.
- 17 J. A. Woodhead, G. R. Rossman and L. T. Silver, *Am. Mineral.*, 1991, **76**, 74–82.
- 18 A. E. Marsellos and J. I. Garver, *Am. Mineral.*, 2010, **95**, 1192–1201.
- 19 G. C. Capitani, H. Leroux, J. C. Doukhan, S. Rios, M. Zhang and E. K. H. Salje, *Phys. Chem. Miner.*, 2000, **27**, 545–556.
- 20 T. Geisler, B. E. Burakov, V. Zirlin, L. Nikolaeva and P. Pöml, *Eur. J. Mineral.*, 2005, **17**, 883–894.
- 21 T. Geisler, M. Zhang and E. K. H. Salje, *J. Nucl. Mater.*, 2003, **320**, 280–291.
- 22 M. Zhang, E. K. H. Salje, G. C. Capitani, H. Leroux, A. M. Clark, J. Schlüter and R. C. Ewing, *J. Phys.: Condens. Matter*, 2000, **12**, 3131–3148.
- 23 T. Geisler, A. M. Seydoux-Guillaume, M. Wiedenbeck, R. Wirth, J. Berndt, M. Zhang, B. Mihailova, A. Putnis, E. K. H. Salje and J. Schlüter, *Am. Mineral.*, 2004, **89**, 1341–1347.
- 24 E. B. Anderson, B. E. Burakov and E. M. Pazukhin, *Radiochim. Acta*, 1993, **60**, 149–151.
- 25 P. C. Burns, R. C. Ewing and A. Navrotsky, *Science*, 2012, **335**, 1184–1188.
- 26 B. E. Burakov, E. B. Anderson, S. I. Shabalev, E. E. Strykanova, S. V. Ushakov, M. Trotabas, J. Y. Blanc, P. Winter and J. Duco, *Mater. Res. Soc. Symp. Proc.*, 1997, **465**, 1297–1308.
- 27 E. M. Pazukhin, *Radiochemistry*, 2008, **50**, 324–331.
- 28 A. A. Shiryaev, I. E. Vlasova, B. E. Burakov, B. I. Ogorodnikov, V. O. Yapaskurt, A. A. Averin, A. V. Pakhnevich and Y. V. Zubavichus, *Prog. Nucl. Energy*, 2016, **92**, 104–118.
- 29 B. E. Burakov, E. B. Anderson, B. Y. Galkin, E. M. Pazukhin and S. I. Shabalev, *Radiochim. Acta*, 1994, **65**, 199–202.
- 30 B. E. Burakov, in *Proceedings of International Conference SAFE WASTE-93*, 1993, vol. 2, pp. 19–28.
- 31 B. E. Burakov, E. E. Strykanova and E. B. Anderson, *Mater. Res. Soc. Symp. Proc.*, 1997, **465**, 1309–1311.
- 32 P. Pöml, B. Burakov, T. Geisler, C. T. Walker, M. L. Grange, A. A. Nemchin, J. Berndt, R. O. C. Fonseca, P. D. W. Bottomley and R. Hasnaoui, *J. Nucl. Mater.*, 2013, **439**, 51–56.
- 33 I. Vlasova, A. Shiryaev, B. Ogorodnikov, B. Burakov, E. Dolgoplova, R. Senin, A. Averin, Y. Zubavichus and S. Kalmykov, *Radiat. Meas.*, 2015, **83**, 20–25.
- 34 T. Kitagaki, K. Yano, H. Ogino and T. Washiya, *J. Nucl. Mater.*, 2017, **486**, 206–215.
- 35 Y. Ohishi, Y. Sun, Y. Ooi and H. Muta, *J. Nucl. Mater.*, 2021, **556**, 153160.
- 36 C. Journeau, Ph.D. Thesis, Université d'Orléans, 2006.
- 37 S. T. Barlow, D. J. Bailey, A. J. Fisher, M. C. Stennett, C. Gausse, H. Ding, V. A. Krasnov, S. Y. Sayenko, N. C. Hyatt and C. L. Corkhill, *npj Mater. Degrad.*, 2020, **4**, 3.
- 38 A. C. Strzelecki, X. Zhao, P. Estevenon, H. Xu, N. Dacheux, R. C. Ewing and X. Guo, *Am. Mineral.*, 2024, **109**, 225–242.
- 39 C. Keller, *Nukleonik*, 1963, **5**, 41–48.
- 40 J. A. Speer, *Rev. Mineral. Geochem.*, 1980, **5**, 113–135.
- 41 J. A. Speer and B. J. Cooper, *Am. Mineral.*, 1982, **67**, 804–808.
- 42 J. M. S. Skakle, C. L. Dickson and F. P. Glasser, *Powder Diffr.*, 2000, **15**, 234–238.
- 43 J. C. Ayers and E. B. Watson, *Philos. Trans. R. Soc., A*, 1991, **335**, 365–375.
- 44 R. C. Newton, C. E. Manning, J. M. Hanchar and R. J. Finch, *J. Am. Ceram. Soc.*, 2005, **88**, 1854–1858.
- 45 M. P. Tole, *Geochim. Cosmochim. Acta*, 1985, **49**, 453–458.
- 46 T. E. Krogh, *Geotimes*, 1995, **40**, 20–22.
- 47 R. C. Ewing, R. F. Haaker and W. Lutze, *Mater. Res. Soc. Symp. Proc.*, 1982, **11**, 389–396.
- 48 D. T. Costin, Ph.D. Thesis, Université de Montpellier 2, 2012.
- 49 S. Szenknect, A. Mesbah, T. Cordara, N. Clavier, H. P. Brau, X. Le Goff, C. Poinssot, R. C. Ewing and N. Dacheux, *Geochim. Cosmochim. Acta*, 2016, **181**, 36–53.
- 50 R. C. Ewing, *Proc. Natl. Acad. Sci. U. S. A.*, 1999, **96**, 3432–3439.
- 51 R. C. Ewing, *Canad. Mineral.*, 2001, **39**, 697–715.
- 52 R. C. Ewing, *C. R. Geosci.*, 2011, **343**, 219–229.
- 53 R. C. Ewing, *Nat. Mater.*, 2015, **14**, 252–257.
- 54 R. C. Ewing, W. Lutze and W. J. Weber, *J. Mater. Res.*, 1995, **10**, 243–246.
- 55 R. C. Ewing, W. J. Weber and W. Lutze, in *Disposal of weapon plutonium*, 1996, pp. 65–83.
- 56 B. E. Burakov and E. B. Anderson, in *Proceedings of International Conference NUCEF'98*, 1990, pp. 295–306.



- 57 B. E. Burakov, E. B. Anderson, B. Y. Galkin, V. A. Starchenko and V. G. Vasiliev, *Disposal of weapons plutonium*, 1996, pp. 85–89.
- 58 B. E. Burakov, E. B. Anderson, V. S. Rovsha, S. V. Ushakov, R. C. Ewing, W. Lutze and W. J. Weber, *Mater. Res. Soc. Symp. Proc.*, 1996, **412**, 33–39.
- 59 B. E. Burakov, J. M. Hanchar, M. V. Zamoryanskaya, V. M. Garbuzov and V. A. Zirilin, *Radiochim. Acta*, 2002, **90**, 95–97.
- 60 E. B. Anderson, B. E. Burakov and L. J. Jardine, *Synthesis of Pu-Doped Ceramic*, Lawrence Livermore National Laboratory, 1998.
- 61 B. D. Begg, N. J. Hess, W. J. Weber, S. D. Conradson, M. J. Schweiger and R. C. Ewing, *J. Nucl. Mater.*, 2000, **278**, 212–224.
- 62 W. Lutze and R. C. Ewing, *Radioactive waste forms for the future*, 1988.
- 63 W. Lutze, R. C. Ewing, K. B. Helean and W. L. Gong, *University of New Mexico report*, 1999.
- 64 W. Lutze, W. L. Gong and R. C. Ewing, *The Environmental Challenges of Nuclear Disarmament*, 2000, pp. 65–74.
- 65 W. J. Weber, R. C. Ewing and W. Lutze, *NATO Workshop on Disposal of Weapons Plutonium*, 1995.
- 66 W. J. Weber, R. C. Ewing and W. Lutze, *Mater. Res. Soc. Symp. Proc.*, 1996, **412**, 25–32.
- 67 S. V. Ushakov, W. L. Gong, M. M. Yagovkina, K. B. Helean, W. Lutze and R. C. Ewing, *Ceram. Trans.*, 1999, **93**, 357–363.
- 68 R. D. Shannon, *Acta Crystallogr., Sect. A: Cryst. Phys., Diffraction, Theor. Gen. Crystallogr.*, 1976, **32**, 751–767.
- 69 R. Caruba, A. Baumer and G. Turco, *Geochim. Cosmochim. Acta*, 1975, **39**, 11–26.
- 70 R. J. Finch and J. M. Hanchar, *Rev. Mineral. Geochem.*, 2003, **53**, 1–25.
- 71 E. D. A. Ferriss, R. C. Ewing and U. Becker, *Am. Mineral.*, 2010, **95**, 229–241.
- 72 S. Labs, *Schriften des Forschungszentrums Jülich*, 2015, p. 267.
- 73 S. Labs, C. Hennig, S. Weiss, H. Curtius, H. Zänker and D. Bosbach, *Environ. Sci. Technol.*, 2014, **48**, 854–860.
- 74 A. Mesbah, S. Szenknect, N. Clavier, J. Lozano-Rodriguez, C. Poinssot, C. Den Auwer, R. C. Ewing and N. Dacheux, *Inorg. Chem.*, 2015, **54**, 6687–6696.
- 75 X. Guo, S. Szenknect, A. Mesbah, S. Labs, N. Clavier, C. Poinssot, S. V. Ushakov, H. Curtius, D. Bosbach, R. C. Ewing, P. C. Burns, N. Dacheux and A. Navrotsky, *Proc. Natl. Acad. Sci. U. S. A.*, 2015, **112**, 6551–6555.
- 76 C. L. Dickson and F. P. Glasser, *Cem. Concr. Res.*, 2000, **30**, 1619–1623.
- 77 P. Estevenon, T. Kaczmarek, F. Vadot, T. Dumas, P. L. Solari, E. Welcomme, S. Szenknect, A. Mesbah, P. Moisy, C. Poinssot and N. Dacheux, *Dalton Trans.*, 2019, **48**, 10455–10463.
- 78 P. Estevenon, E. Welcomme, S. Szenknect, A. Mesbah, P. Moisy, C. Poinssot and N. Dacheux, *Dalton Trans.*, 2019, **48**, 7551–7559.
- 79 A. C. Strzelecki, C. Bourgeois, K. W. Kriegsman, P. Estevenon, N. Wei, S. Szenknect, A. Mesbah, D. Wu, R. C. Ewing, N. Dacheux and X. Guo, *Inorg. Chem.*, 2020, **59**, 13174–13183.
- 80 C. Frondel and R. L. Collette, *Am. Mineral.*, 1957, **42**, 759–765.
- 81 F. A. Mumpton and R. Roy, *Geochim. Cosmochim. Acta*, 1961, **21**, 217–238.
- 82 S. V. Ioudintsev, B. I. Omelianenko and M. I. Lapina, *Mater. Res. Soc. Symp. Proc.*, 1998, **506**, 185–189.
- 83 T. Barral, P. Estevenon, Y. Chanteau, T. Kaczmarek, A. C. Strzelecki, D. Menut, E. Welcomme, S. Szenknect, P. Moisy, X. Guo and N. Dacheux, *Dalton Trans.*, 2023, **52**, 10023–10037.
- 84 N. Dacheux, V. Brandel and M. Genet, *New J. Chem.*, 1995, **19**, 15–25.
- 85 R. K. Iler, *The chemistry of silica: solubility, polymerization, colloid and surface properties, and biochemistry*, John Wiley & Sons, Hoboken, NJ, 1979.
- 86 N. Clavier, S. Szenknect, D. T. Costin, A. Mesbah, J. Ravoux, C. Poinssot and N. Dacheux, *J. Nucl. Mater.*, 2013, **441**, 73–83.
- 87 C. Frontera and J. Rodriguez-Carvajal, *Phys. B*, 2003, **335**, 219–222.
- 88 J. Schindelin, I. Arganda-Carreras, E. Frise, V. Kaynig, M. Longair, T. Pietzsch, S. Preibisch, C. Rueden, S. Saalfeld, B. Schmid, J.-Y. Tinevez, D. J. White, V. Hartenstein, K. Eliceiri, P. Tomancak and A. Cardona, *Nat. Methods*, 2012, **9**, 676–682.
- 89 R. J. Finch, J. M. Hanchar, P. W. O. Hoskin and P. C. Burns, *Am. Mineral.*, 2001, **86**, 681–689.
- 90 L. H. Fuchs and E. Gebert, *Am. Mineral.*, 1958, **43**, 243–248.
- 91 P. Dawson, M. M. Hargreave and G. R. Wilkinson, *J. Phys. C: Solid State Phys.*, 1971, **4**, 240–256.
- 92 A. C. Strzelecki, T. Barral, P. Estevenon, A. Mesbah, V. Goncharov, J. Baker, J. Bai, N. Clavier, S. Szenknect, A. Migdisov, H. Xu, R. C. Ewing, N. Dacheux and X. Guo, *Inorg. Chem.*, 2021, **60**, 718–735.
- 93 N. Clavier, S. Szenknect, D. T. Costin, A. Mesbah, C. Poinssot and N. Dacheux, *Spectrochim. Acta, Part A*, 2014, **118**, 302–307.
- 94 H. Weitzel and C. Keller, *J. Solid State Chem.*, 1973, **13**, 136–141.

